



**HAL**  
open science

## Mechanical properties of breast, kidney, and thyroid tumours measured by AFM: relationship with tissue structure

Aurélie Levillain, Cyrille Confavreux, Myriam Decaussin-Petrucci, Emeline Durieux, Philippe Paparel, Karine Le-Bail Carval, Laure Maillard, François Bermond, David Mitton, Hélène Follet

### ► To cite this version:

Aurélie Levillain, Cyrille Confavreux, Myriam Decaussin-Petrucci, Emeline Durieux, Philippe Paparel, et al.. Mechanical properties of breast, kidney, and thyroid tumours measured by AFM: relationship with tissue structure. *Materialia*, 2022, 25, pp.101555. 10.1016/j.mtla.2022.101555 . hal-03765624

**HAL Id: hal-03765624**

**<https://hal.science/hal-03765624v1>**

Submitted on 31 Aug 2022

**HAL** is a multi-disciplinary open access archive for the deposit and dissemination of scientific research documents, whether they are published or not. The documents may come from teaching and research institutions in France or abroad, or from public or private research centers.

L'archive ouverte pluridisciplinaire **HAL**, est destinée au dépôt et à la diffusion de documents scientifiques de niveau recherche, publiés ou non, émanant des établissements d'enseignement et de recherche français ou étrangers, des laboratoires publics ou privés.

## Journal Pre-proof

Mechanical properties of breast, kidney, and thyroid tumours measured by AFM: relationship with tissue structure

A. Levillain , C.B. Confavreux , M. Decaussin-Petrucci ,  
E. Durieux , P. Paparel , K. Le-Bail Carval , L. Maillard ,  
F. Bermond , D. Mitton , H. Follet

PII: S2589-1529(22)00237-X  
DOI: <https://doi.org/10.1016/j.mtla.2022.101555>  
Reference: MTLA 101555



To appear in: *Materialia*

Received date: 17 June 2022  
Accepted date: 26 August 2022

Please cite this article as: A. Levillain , C.B. Confavreux , M. Decaussin-Petrucci , E. Durieux , P. Paparel , K. Le-Bail Carval , L. Maillard , F. Bermond , D. Mitton , H. Follet , Mechanical properties of breast, kidney, and thyroid tumours measured by AFM: relationship with tissue structure, *Materialia* (2022), doi: <https://doi.org/10.1016/j.mtla.2022.101555>

This is a PDF file of an article that has undergone enhancements after acceptance, such as the addition of a cover page and metadata, and formatting for readability, but it is not yet the definitive version of record. This version will undergo additional copyediting, typesetting and review before it is published in its final form, but we are providing this version to give early visibility of the article. Please note that, during the production process, errors may be discovered which could affect the content, and all legal disclaimers that apply to the journal pertain.

© 2022 Published by Elsevier B.V. on behalf of Acta Materialia Inc.

## Mechanical properties of breast, kidney, and thyroid tumours measured by AFM: relationship with tissue structure

A. Levillain (1,2), C.B. Confavreux (1,3,4), M. Decaussin-Petrucci (3,5,6), E. Durieux (7), P. Paparel (3), K. Le-Bail Carval (8), L. Maillard (9), F. Bermond (2), D. Mitton (2), H. Follet (1)

1. Univ Lyon, Univ Claude Bernard Lyon 1, INSERM, LYOS UMR 1033, Lyon, France; 2. Univ Lyon, Univ Gustave Eiffel, Univ Claude Bernard Lyon 1, LBMC UMR\_T 9406, F-69622 Lyon, France; 3. Hospices Civils de Lyon, Centre hospitalier Lyon Sud, Pierre Bénite, France; 4. Centre Expert des Métastases Osseuses et Oncologie Osseuse Secondaire –CEMOS-, Service de Rhumatologie, Institut de Cancérologie des Hospices Civils de Lyon (IC-HCL), Lyon, France; 5. Service d'Anatomo-Pathologie, Hospices civils de Lyon, France; 6. Univ Claude Bernard Lyon 1, EA 3738 CICLY, Oullins, France; 7. Centre de Pathologie et de Neuropathologie Est, Lyon, France ; 8. CHU Lyon Est, hopital femme mere enfant, departement de gynecologie-obstetrique, Univ Claude Bernard Lyon 1, 69000 Lyon, France ; 9. Service de Chirurgie Endocrinienne, Centre Hospitalier Lyon Sud, Hospices Civils de Lyon, 69495 Pierre-Benite, France

Corresponding author:

Hélène Follet

INSERM, Université de Lyon, UMR1033

Faculte de Medecine Lyon Est -Domaine Laennec-6th

7-11, rue G. Paradin

69372 Lyon cedex 08, France

+33 4 78 78 57 26

[helene.follet@inserm.fr](mailto:helene.follet@inserm.fr)

### Graphical abstract



**Abstract**

The mechanical properties of the extracellular matrix are essential for regulating cancer cell behaviour, but how they change depending on tumour type remains unclear. The aim of the current study was to determine how the mechanical properties of tumours that frequently metastasize to bones were affected depending on histological type. Human breast, kidney, and thyroid specimens containing tumour and normal tissue were collected during surgery. The elastic modulus and elastic fraction of each sample were characterised using atomic force microscopy and compared with histopathological markers. We observed that tumour mechanical properties were differentially affected depending on organ and histological type. Indeed, clear cell renal carcinoma and poorly differentiated thyroid carcinoma displayed a decrease in the elastic modulus compared to their normal counterpart, while breast tumours, papillary renal carcinoma and fibrotic thyroid tumours displayed an increase in the elastic modulus. Elastic fraction decreased only for thyroid tumour tissue, indicating an increase in viscosity. These findings suggest a unique mechanical profile associated with each subtype of cancer. Therefore, viscosity could be a discriminator between tumour and normal thyroid tissue, while elasticity could be a discriminator between the subtypes of breast, kidney and thyroid cancers.

**Keywords:** Tumour, Atomic Force Microscopy, Viscoelasticity, Extracellular Matrix

## 1. Introduction

Bone metastases occur in more than 1.5 million cancer patients worldwide, and are associated with serious skeletal-related events, including pathological fracture, pain, disability, and spinal cord compression (1, 2). Patient-specific finite element models of metastatic bone are a promising tool to predict the fracture risk of patients (3). However, the accuracy of such models is hampered by several limitations, including a limited knowledge of metastatic bone mechanical properties. Bone metastases can come from various primary cancers, therefore, knowledge of tumour mechanical properties from different types of cancer can provide valuable information for the model. Moreover, a characterisation of tumour mechanical properties could help for (a) developing biomimetic biomaterials to elucidate the role of stiffness and viscosity for metastatic spread, and (b) improve cancer diagnosis using *in vivo* imaging. The most common cancers to metastasize to bone are breast, prostate, thyroid, lung, and kidney cancers (4). The ability of cancer cells to metastasize mainly depends on the physical interactions and mechanical forces between these cells and the microenvironment they migrate through. In particular, the extracellular matrix (ECM) plays a crucial role in metastatic spread. The ECM has unique physical, biochemical, and biomechanical properties that are essential for regulating cell behaviour. During cancer progression, the ECM undergoes extensive remodelling (5) and its stiffness plays a causative role in cancer pathogenesis (6). In breast, a stiffer ECM stimulates epithelial-like cell transformation from normal cells to malignant cells with a more aggressive phenotype that promotes cancer cell invasion (5, 7). However, although several studies have been conducted on the mechanical characterisation of breast tumour at the tissue level (8–11), there is a lack of knowledge regarding the mechanical properties of tumours from other tissues, including thyroid and kidney.

Several lines of evidence suggest that the extent of mechanical alterations depends on the type of tumour. First, while most studies on breast cancer have shown that tumour tissue exhibited an increase in stiffness compared to normal tissue (8, 10, 12, 13), a study using a palpation device to measure tissue elasticity showed that renal cell carcinoma tissue was softer than normal kidney tissue (14). Differences in mechanical alterations between tumour and normal tissue have also been

observed for the same organ. In their study characterising the mechanical properties of breast tissue samples from different types, Samani *et al* found that the increase in the elastic modulus was dependent on the tumour type, with high-grade invasive ductal carcinoma exhibiting the highest increase compared to normal tissue (10). Similarly, the elastic modulus of thyroid tumour tissue is differentially affected depending on the type of cancer, with samples of papillary carcinoma exhibiting a significantly higher elastic modulus compared to normal thyroid tissue, while samples of follicular adenocarcinoma exhibit a similar stiffness compared to normal thyroid tissue (15). Second, *in vitro* studies demonstrated that a rigidity profile is an intrinsic property of each cancer line; some cells display increased growth as ECM rigidity increases, while some cancer cells grow equally well across a large spectrum of ECM rigidity (16). This finding suggests that cancer spread depends both on ECM mechanical properties and on the tumour type. Therefore, it is important to characterise the mechanical properties of a tumour along with its histological type. However, a direct comparison from the literature regarding the mechanical properties of different types of tumours is challenging, because most studies focused on one type of tissue and the characterisation techniques varied among the studies. More specifically, there is variability in the length scales between the different characterisation techniques, from tissue-level (8, 11) to tumour-level (10, 12, 13, 15). A characterisation of the tumours at the tissue level is more relevant in order to (a) account for potential heterogeneity of the tumour and (b) to uncover the mechanobiology mechanisms of cancer progression and metastatic spread.

Indentation using atomic force microscopy (AFM) has been used to reveal the nanomechanical signature of human breast (8, 11), liver (17), brain (18), ovarian (19), and prostate (20) cancer. Mapping of the elastic modulus in breast tumour tissue at two different stages of cancer progression highlighted different stiffness profiles, with malignant tissues showing a broader distribution of Young's modulus compared to normal and benign tissues (8). This finding emphasizes the ability of AFM to reveal differences in elastic properties according to cancer progression, and suggests that it could also reveal differences according to tumour type. To date, most research on the mechanical properties of tumour

tissue has focused on elasticity as the key determinant of tissue behaviour. Yet, ECM exhibits both elastic and viscous properties, and changes in ECM viscoelasticity affects cell activities (21). For example, a decrease in collagen fibers' stress relaxation is associated with a reduction of cell persistent migration (22). This highlights the need to account for both the elastic and viscous properties of a tumour. In recent years, there have been significant development in measuring the viscoelastic properties of soft tissues using AFM (23). This technique has the potential to reveal the viscoelastic properties of tumour tissue, which can then be correlated with histopathological markers.

The aim of this study was to determine how the mechanical properties of tumour tissues that frequently metastasize to bone are affected depending on their histological type. Based on the findings for breast tumours (8, 10), it was first hypothesized that the elastic properties of tumours are differentially affected depending on their type. Second, given the role of ECM viscoelasticity in regulating cell and tissue dynamics (21), it was hypothesized that tumour tissue exhibits a change in viscous properties compared to normal tissue. To test these hypotheses, we characterised the elastic and viscoelastic properties of breast, kidney and thyroid tumour tissues using AFM, and we compare them with histopathological markers.

## 2. Materials and methods

### 2.1 Study participants and tissue preparation

The study protocol was approved by the French Ethics Committee (CPP SUD-EST 1 France) under registration number ID-RCB: 2019-A01202-55. All procedures have been conducted in compliance with national and European regulations. All included patients received clear information and provided written consent. Human breast (n=6), kidney (n=5), and thyroid (n=4) specimens containing tumour tissue were collected post-surgery at Hospices Civils de Lyon (Groupement Hospitalier Est (KLBC) and Hôpital Lyon Sud (LM, PP), France). From each removed specimen, the pathologist prepared one sample containing healthy and tumour tissue (breast) or one healthy tissue sample and one tumour tissue sample (kidney and thyroid) for AFM testing. The samples used for AFM were free of necrotic areas and their dimensions were at least 2 x 10 x 10 mm. The remaining specimen was used for routine pathological diagnosis. The samples used for AFM testing were immediately frozen at -80°C and stored at this temperature until the day of experiment.

### 2.2 Histopathological examination

Samples used for pathological diagnosis were fixed in formol and embedded in paraffin. 3 µm-thick sections were cut using a microtome and stained with hematoxylin eosin saffron. Connective tissue (collagen) was stained in yellow, while muscle and cytoplasm were stained in pink. For each sample, one section containing tumour tissue was imaged in transmitted illumination using a light microscope. Histopathological examination was performed by expert pathologists and included assessing the type of carcinoma and extent of fibrosis.

### 2.3 AFM testing

Frozen samples were carefully cut using a scalpel to obtain a 2-3 mm thick slice, with smooth and uniform surfaces. On the day of experiment, samples were thawed at room temperature for 1 hour, glued on a petri dish and immersed in phosphate buffered saline (PBS). Mechanical manipulations during sample preparation were always kept minimal. The samples were then allowed to set for 30 minutes to avoid swelling of the sample during AFM testing. The petri dish was placed on the AFM

stage and tests were carried out at room temperature (Figure 1A). AFM tests were performed using a Nanowizard3 AFM (JPK Instruments AG, Germany) equipped with Silicon nitride cantilevers (MLCT, Bruker) and a pyramidal shaped tip. Two cantilevers were used depending on the stiffness of the sample; their nominal spring constant was 0.01 (MLCT-C) and 0.03 (MLCT-D) N/m, respectively. The cantilever spring constant was calibrated using the method described in (24) and the deflection sensitivity was determined using the standardized nanomechanical AFM procedure (25).

For each sample, three random regions at least 1 mm apart were probed over a 100  $\mu\text{m}$  x 100  $\mu\text{m}$  area, with three force maps performed in each region. Since the samples could display high topography, which would have a non-negligible effect on the measurements (26), a two-step method was followed (27). First, tapping mode topography was used to identify a 15  $\mu\text{m}$  x 15  $\mu\text{m}$  zone of interest with minimal slope (Figure 1B). Second, force-displacement curves were recorded at 3  $\mu\text{m}$  spacing intervals over the zone of interest (25 curves), following a trapezoidal loading profile. The loading segment (extend) was carried out at 2  $\mu\text{m}/\text{s}$  until a force of 0.3-0.5 nN was reached. The value of the maximal force was adjusted for each sample in order to have an indentation within the range of 300-1500  $\mu\text{m}$ . The maximal force was then held constant for 1 s and the unloading segment (retract) was carried out at 10  $\mu\text{m}/\text{s}$ . The range of the force displacement curve was 7  $\mu\text{m}$  to correct the baseline. For each sample, measurement of the mechanical properties was performed within two hours to prevent biochemical changes in the tissue (11).

#### 2.4 Elastic and viscoelastic analysis

From the raw data (Vertical deflection as a function of piezo height), force-indentation curves were obtained using JPK Data Processing software (v.6.1.163, JPK Instruments AG). The baseline offset and linear fit of the tilt were subtracted from the vertical deflection. If the baseline could not be linearly fitted (e.g., due to a bubble or a particle floating in the medium), the curve was excluded. The contact point, defined as the first crossing of the y axis (vertical deflection), was then identified and the piezo

height offset was adjusted. Indentation was calculated by subtracting the cantilever deflection from the piezo height.

Elastic and viscoelastic analyses were then performed from the force-indentation curve and the Indentation-time curve, respectively. For the elastic analysis, the Hertz-Sneddon model for a four-sided pyramid was used, where the **elastic modulus, E**, is defined by equation 1 (28).

$$F = \frac{E}{1 - \nu^2} \frac{\tan(\alpha)}{\sqrt{2}} \delta^2 \quad (1)$$

Where F is the force,  $\delta$  is the indentation,  $\nu$  is Poisson's ratio and  $\alpha$  is the face angle of the four-sided pyramid. The elastic modulus represents the stiffness of the material. A Poisson's ratio of 0.5 was chosen assuming the incompressibility of soft biological tissues. The elastic modulus was derived using Equation 1 by fitting the force-indentation curves using E and the contact point as fit parameters. Curves with low quality fit ( $R^2 < 0.98$ ) were discarded. Moreover, for each dataset (one dataset per sample), outliers, defined as values deviating from the mean by more than three standard deviations, were excluded from the analysis.

For the viscoelastic analysis, the standard linear solid (SLS) model was used. The solution for spherical indentation was adapted for indentation with a pyramidal tip (29). Briefly, using the elastic-viscoelastic correspondence, equation 1 becomes:

$$\delta^2 = \frac{1}{\sqrt{2} \tan(\alpha)} \int_0^t J(t-u) \frac{dF}{du} du \quad (2)$$

Where u is the dummy variable of integration for time and J(t) is the creep function.

For the SLS model, the creep function is defined as:

$$J(t) = C_0 - C_1 \exp\left(\frac{-t}{\tau_1}\right) \quad (3)$$

Where  $C_0$ ,  $C_1$ , and  $\tau_1$  are model parameters.

For a ramp from zero load at a ramp rate  $dP/dt = k$ , the solution of equation 2 is:

$$\delta^2 = \begin{cases} \frac{k}{\sqrt{2} \tan(\alpha)} (C_0 t - C_1 \tau_1 [1 - \exp(\frac{-t}{\tau_1})]), & 0 \leq t \leq t_r \\ \frac{k}{\sqrt{2} \tan(\alpha)} (C_0 t_r - C_1 \tau_1 \exp(\frac{-t}{\tau_1}) [\exp(\frac{t_r}{\tau_1}) - 1]), & t > t_r \end{cases} \quad (4)$$

The model parameters were derived using equation 4 by fitting the indentation-time curve on the holding segment. Curves with low quality fit ( $R^2 < 0.95$ ) were discarded.

The instantaneous modulus,  $E_{ins}$ , the equilibrium modulus,  $E_{eq}$ , and the **elastic fraction,  $f$** , which quantifies the extent of viscous behaviour of the material (30, 31), (with an elastic fraction of 0 representing a purely elastic material, and an elastic fraction of 1 representing a purely viscous material) were then calculated as:

$$E_{ins} = \frac{1 + \nu}{C_0 - C_1} \quad (5)$$

$$E_{eq} = \frac{1 + \nu}{C_0} \quad (6)$$

$$f = \frac{E_{eq}}{E_{ins}} \quad (7)$$

## 2.5 Statistical analysis

Statistical analyses were performed in Python. For each sample, a statistical comparison between normal and tumour tissue was made on the total number of indents. Normal distribution was tested using Shapiro test with an alpha risk of 0.05. A Mann-Whitney test was used to compare between normal and tumour tissues the elastic modulus and the elastic fraction with a level of significance of 0.05.

### 3. Results

#### 3.1 Mechanical properties and structure of breast tumours

Breast tumour samples were composed of invasive breast carcinoma of no special type (NST) (n=3) and invasive lobular carcinomas (ILC) (n=3) (Figure 3). Mean and median values of elastic modulus and elastic fraction for each sample are reported in Table 1. The elastic modulus of tumour tissue significantly increased compared to its normal counterpart in 5 out of 6 samples, with mean values of  $1.4 \pm 0.91$  kPa in control and  $3.3 \pm 3.4$  kPa in tumour tissue for NST, and  $1.2 \pm 0.29$  kPa in control and  $2.8 \pm 1.5$  kPa in tumour tissue for ILC (Figure 3A, Table 1). No particular trend was observed in the elastic fraction between normal and tumour tissue, with mean values of  $0.53 \pm 0.069$  in control and  $0.53 \pm 0.047$  in tumour tissue (Figure 3B, Table 1). Only one sample displayed a significant increase in the elastic fraction in tumour tissue. NST samples displayed a well-defined tumour mass within the adipose tissue (Figures 3C-D), while ILC samples displayed a more diffuse tumour mass (Figures 3E-F). Both types exhibited an extensive fibrotic stroma (Figures 3D, F – arrows).

#### 3.2 Mechanical properties and structure of kidney tumours

We obtained five kidney tumour samples composed of clear cell renal cell carcinomas (RCC) (n=3), papillary RCC (n=1) and a mix between clear cell RCC and sarcomatoid (n=1) (Figure 4). Mean and median values of elastic modulus and elastic fraction for each sample are reported in Table 2. Elastic modulus of tumour tissue significantly decreased compared to its normal counterpart for all clear cell RCC samples, with mean values of  $3.2 \pm 2.7$  kPa in control and  $1.7 \pm 1.6$  kPa in tumour tissue (Figure 4A). The elastic fraction was similar between normal (mean value:  $0.48 \pm 0.14$ ) and tumour (mean value:  $0.52 \pm 0.021$ ) tissue, with only one sample showing a significant decrease in tumour tissue. Tumour tissue exhibited a high cellular density with little fibrotic tissue (Figures 4C, G) compared to normal tissue, which is composed of renal tubes (Figure 4F – asterisks) surrounded by connective tissue (Figure 4F – arrowheads). The papillary RCC sample displayed a significant increase in the elastic modulus in tumour tissue compared to normal tissue, with a high heterogeneity in tumour tissue (Figure 4A, Table 2). The mean elastic modulus was  $67 \pm 138$  kPa in tumour and  $3.0 \pm 4.5$  kPa in control

tissue. No significant difference was observed in the elastic fraction between normal and tumour tissue. Cancer cells were packed in a papillary architecture and surrounded by fibrotic tissue (Figures 4D, H – arrow). The sample with a mix of clear cell and sarcomatoid RCC showed a high heterogeneity in the elastic properties in tumour tissue, with a mean elastic modulus of  $15 \pm 36$  kPa (Figure 4A, Table 2). No significant difference was observed in the elastic modulus and elastic fraction between normal and tumour tissue (Figure 4B, Table 2). This sample exhibited a high cellular density with little fibrotic tissue in the clear cell carcinoma area, and elongated cells surrounded by a fibrotic stroma in the sarcomatoid carcinoma area (Figures 4E, I – arrows).

### 3.3 Mechanical properties and structure of thyroid tumours

Thyroid tumour samples were composed of papillary (n=1), anaplastic (n=1) and poorly differentiated (n=1) carcinomas, with one additional sample exhibiting papillary and anaplastic types. Mean and median values of elastic modulus and elastic fraction for each sample are reported in Table 3. The papillary carcinoma and anaplastic samples displayed a significantly increased elastic modulus in tumour tissue compared to their normal counterpart, with mean values of  $0.54 \pm 0.28$  kPa in control and  $1.7 \pm 1.7$  kPa in tumour tissue for papillary carcinoma, and  $1.3 \pm 1.0$  kPa in control and  $2.4 \pm 2.2$  kPa in tumour tissue for anaplastic carcinoma (Figure 5A, Table 3). The papillary carcinoma sample also displayed a decrease in the elastic fraction in tumour tissue, while no difference was observed for the anaplastic carcinoma sample. In both samples, cancer cells were surrounded by an extensive fibrotic stroma (Figure 5D-E, I-J – arrows), while normal thyroid tissue was mainly composed of colloid fluid (Figure 5H – asterisks) and follicular cells, surrounded by little connective tissue (Figure 5H – arrowheads). The papillary/anaplastic and poorly differentiated samples displayed a significantly decreased elastic modulus in tumour tissue compared to its normal counterpart, with mean values of  $1.4 \pm 1.6$  kPa in control and  $0.070 \pm 0.056$  kPa in tumour tissue for papillary/anaplastic carcinoma, and  $2.9 \pm 2.5$  kPa in control and  $0.78 \pm 0.54$  kPa in tumour tissue for poorly differentiated carcinoma (Figure 5A, Table 3). Both samples exhibited a high cellular density with little fibrotic tissue (Figure 5E-G, K-L).

#### 4. Discussion

In the present study, we showed that the elastic and viscoelastic properties of tumour tissue were differentially affected depending on the organ and on the structure and composition of the tissue. The first hypothesis, that the elastic properties of the tumours were differentially affected depending on their type, was corroborated. Clear cell renal carcinoma and poorly differentiated thyroid carcinoma displayed a decrease in the elastic modulus compared to their normal counterpart, while breast tumours, papillary renal carcinoma and fibrotic thyroid tumours displayed an increase in the elastic modulus. The second hypothesis, that tumour tissue exhibits a change in viscous properties compared to normal tissue, was partially corroborated. While the elastic fraction of thyroid tumour tissue tended to be lower compared to their normal counterpart, indicating an increase in viscosity, no consistent difference was observed for breast and kidney tissue. These findings suggest a unique mechanical profile associated with each subtype of cancer.

The present study emphasizes the potential of AFM to characterise tissue mechanical properties of different types of tumours. We developed a method to identify both elastic and viscoelastic properties, providing new valuable information for the development of biomaterials mimicking the mechanical properties of the tumour microenvironment. Indentation tests using AFM were performed on intact samples, without any processing to make the surface smooth or to level the sample. The surface tomography obtained prior to the tests ensured that the slope and the surface irregularities on the zone of interest were kept minimal. The elastic modulus of breast tissues obtained using this protocol was in agreement with other studies using AFM (8, 11). For example, our mean values of elastic modulus for normal (1.4 kPa) and tumour (3.3 kPa) breast tissues were consistent with the study of Plodinec *et al.*, who obtained peak stiffness values of 1.13 to 1.83 kPa for healthy tissue, and 1.54 to 9.62 kPa for malignant breast tumour tissue (8). For the elastic fraction, the values for tumour breast tissue obtained in our study ranged between 0.48 and 0.60 and were higher than the values obtained in Qiu *et al.*, which ranged between 0.15 and 0.38. However, in their study, Qiu *et al* characterized the

viscoelastic properties of tumour tissue obtained after subcutaneously injecting breast cancer cells in a murine model (32). Therefore, the differences in the microenvironment between breast and subcutaneous tissues can explain the different mechanical properties between both tumour tissues. To our knowledge, the mechanical properties of thyroid and kidney tumour tissues had not been characterised using AFM. Although the elastic modulus values found in our study were lower than the values obtained using compression testing (15), shear wave elastography (SWE) (33), or palpation device technique (14), which can be explained by the different measurement scales, the comparison between healthy and tumour tissue was consistent with the literature. Lee *et al.* found that clear cell renal cell carcinoma tissues displayed a decrease in their elastic modulus compared to benign tissue, with mean values of  $13.0 \pm 8.2$  kPa and  $19.2 \pm 10.8$  kPa, respectively (14). For thyroid tissue, measurements at the macroscopic scale revealed a higher elastic modulus of papillary tumour tissue compared to normal tissue (15, 33), which is consistent with our findings.

The results of this study suggest that the mechanical properties of tumour tissues are differentially affected depending on their type and subtype, and that the stiffness of tumour tissue is directly associated with ECM remodelling. Breast tumour tissues displayed a dense fibrotic stroma, resulting in a significant increase in the elastic modulus, which was twice to three times higher than the elastic modulus of normal breast samples. This increase in the elastic modulus seemed to be stronger for NST samples, which were characterised by a well-defined and dense tumour mass, compared to ILC samples. Similarly, papillary renal carcinoma, papillary and anaplastic thyroid tumours exhibited a fibrotic stroma, associated with an increase in the elastic modulus compared to their normal counterpart. Tumour fibrosis is a well-known feature associated with cancer progression and stiffening of the stroma (34). Indirectly, we previously observed that phenomenon in our POU MOS cohort with periostin, a marker of ECM reaction that was associated with survival in bone metastatic adenocarcinoma lung cancer patients (35). The disruption of the balance between ECM synthesis and enzymatic degradation in favour of ECM synthesis has been primarily attributed to the inability of matrix metalloproteinases (MMPs) to digest collagen and alteration of the mode of collagen cross-

linking (36). By contrast, clear cell renal carcinoma and poorly differentiated thyroid carcinoma displayed a high cellular density, which was associated with a decrease in the elastic modulus by at least 50%. Further investigation at the tissue and molecular level will be necessary to elucidate the mechanisms behind this imbalance of ECM remodelling in favour of enzymatic degradation. Altogether, these findings suggest specific processes by which cancer cells alter the structure and composition of tumour tissue, resulting in a different effect on the mechanical properties of the tissue. The type of changes associated with each cancer likely affects cancer progression and metastasis formation.

Several studies suggest a link between the mechanical properties of breast tumours and their metastatic potential and aggressiveness. In particular, it has been shown using a mouse model of breast cancer that tissue stiffening can promote bone metastasis (37). Similarly, several studies indicated a positive correlation between breast cancer aggressiveness and tissue stiffening at the macroscale (10) and tissue scale (38). The relationships between tumour stiffness and its metastatic potential and aggression have not been investigated for thyroid and kidney cancer. Our findings suggest different conclusions than for breast tissue. Indeed, we found that poorly differentiated thyroid and anaplastic carcinomas, respectively, which are very aggressive and frequently metastasise to bone and lung (39, 40), follow different trends, with either a reduced or increased elastic modulus compared to their normal counterpart, respectively. Moreover, we showed that clear cell renal carcinomas, which have the highest metastatic potential (41), display a reduced elastic modulus, while papillary carcinoma displays an increased elastic modulus. Therefore, the relationships between tissue stiffness and cancer aggressiveness and metastatic potential merit further investigation for thyroid and kidney cancer.

Our study also provides new knowledge on the viscoelastic properties of tumour tissue. Although the viscous properties of the ECM are known to play a role in cell activities, very few studies have characterised the viscoelastic properties of tumour tissue. In their *in vivo* study investigating the

viscoelastic shear properties of pathological breast tissue using magnetic resonance elastography (MRE), Sinkus *et al.* showed that shear modulus was a better parameter than viscosity at differentiating between benign and malignant lesions (42). Moreover, they found two clusters of breast cancer, one of which was as viscous as the surrounding tissue. Conversely, Garteiser *et al.* found that the loss modulus of liver tumours measured using MRE, which represents the viscous behaviour of the tissue, was a better discriminator between benign and malignant tumours than storage modulus, which represents elastic behaviour (43). These findings demonstrate that the type of viscoelastic change allowing the discrimination between benign and malignant tumours depend on the tissue. Similarly, in our study at the tissue level, we found discrepancies in the viscoelastic changes between normal and tumour tissues depending on the type of cancer. While breast and kidney tumours did not exhibit any consistent difference in their elastic fraction compared to their surrounding normal tissue, thyroid tumour tissues tended to be more viscous than their surrounding normal tissue. Therefore, viscosity could be a discriminator between tumour and normal thyroid tissue, while elasticity could be a discriminator between the subtypes of cancer.

The current study presents several limitations. First, the robustness of the results is limited by the small sample size, which is mainly due to the difficulty in obtaining tissue from specific subtypes of cancer. In particular, some cancer types are rare (sarcomatoid renal carcinoma, anaplastic and poorly differentiated thyroid carcinomas), and only one sample for each of these types could be obtained. Our findings will have to be confirmed with more samples. However, this study is a proof of concept that is a good starting point for further investigation. Second, due to logistic reasons, the samples were frozen before their mechanical characterisation. There is no consensus on the literature as to whether freezing affects the mechanical properties of biological soft tissues. Indeed, some studies showed that there is not any significant difference in the stiffness between fresh and frozen tissues (44–47), while other studies found an increase (48) or a decrease (49) in the stiffness of frozen tissue compared to fresh tissue. This discrepancy in the effect of freezing can be explained by the different freezing protocols used, in terms of temperature (-20°C or -80°C), number of freezing cycles and duration of

freezing. Comparison of various freezing protocols on soft tissues demonstrated that one or two freezing cycles at  $-80^{\circ}\text{C}$  for up to three months did not result in any significant difference in Young's modulus compared to fresh tissue, while storage at  $4^{\circ}\text{C}$  for more than 24 hours resulted in a decreased Young's modulus (45, 47, 50). Moreover, preservation of histological integrity was better for tissue frozen once at  $-80^{\circ}$  compared to  $-20^{\circ}\text{C}$  (45). The elastic modulus of breast tissue obtained in our study were in agreement with the values obtained on fresh tissue (8, 11), suggesting that freezing did not significantly alter the mechanical properties of these tumour tissues. Moreover, we proposed a comparative study with the same conservation mode for all the tissues. Third, the entire tumour could not be characterised because a part of the tumour was used for clinical diagnosis. The location of the sample used for AFM within the tumour could vary and potentially induced variability in the mechanical properties. To account for this limitation, several measurements were performed in each sample to cover a large area. Fourth, since the current study focused on the mechanical properties of tumour tissues, assessment of tissue structure using histology has not been performed on the same samples. Future studies will aim to spatially correlate tissue structure and mechanical properties by performing AFM and histology on the same samples, following cryosectioning for example (51). Moreover, an investigation at the ultra-structural and molecular scales needs to be done to understand the mechanisms of how the mechanical properties of each type of tumour are differentially affected.

From a clinical perspective, our findings on the mechanical properties of tumour tissue have the potential to significantly advance the field of cancer research and have implications for diagnosis purposes. First, the range of elastic moduli of tumour tissue from various cancers can help improve the accuracy of the failure load predicted by finite element models of metastatic bones. Second, a recent study developing hydrogels mimicking the heterogeneous mechanical properties of breast tumour showed how stiffness regulates pro-metastatic functions of breast cancer cells, both *in vitro* and *in vivo* (52). The range of elastic moduli found in our study for breast, kidney, and thyroid tumour tissue, which will need to be confirmed with the characterisation of fresh samples and with a higher sample size, could allow the development of similar biomaterials, in order to elucidate the role of stiffness and

viscosity for metastatic spread depending on cancer subtype. Third, with the progress of *in vivo* imaging techniques to characterise the viscoelastic properties of soft tissues with a higher spatial resolution, namely SWE (53) and microscopic Magnetic Resonance Elastography (MRE) (54–56), the mechanical properties of a tumour could then be used as an *in vivo* predictive marker of bone metastasis formation.

In conclusion, this study brought new insights regarding the modification of viscoelastic properties of tumour tissue in different types of cancer. While we found that the elastic modulus of breast tumour tissue increased compared to normal surrounding tissue, various effects were observed for kidney and thyroid tissue depending on the type, structure and composition of the tumour. The elastic fraction of tumour tissue decreased only for the thyroid, suggesting a role of viscosity for thyroid cancer progression. These findings on different types of cancer form a first basis to: (a) implement the mechanical properties of different types of tumours in finite element models and (b) understand how mechanical alterations are linked to aggressiveness and metastatic potential of cancer. For this latter point, a characterisation of the elasticity of cancer cells could be performed and correlated with cell activities. Identification of mechanical parameters predictive of cancer progression will have implications for diagnosis purposes.

#### **Declaration of interests**

The authors declare that they have no known competing financial interests or personal relationships that could have appeared to influence the work reported in this paper.

## 5. Acknowledgments

We thank Corinne Perrin and Karine Castellano from Hospices Civils de Lyon for specimen collection, Sara Calattini and Mélanie Roche from Cancer Institute Research Platform of Hospices Civils de Lyon (IC-HCL) for coordinating the clinical study. We also acknowledge the contribution of SFR Biosciences (UAR3444/CNRS, US8/Inserm, ENS de Lyon, UCBL) facilities and the staff of Platim, especially Simone Bovio for his help with AFM. This study has received funding from the European Union's Horizon 2020 research and innovation programme under the Marie Skłodowska-Curie grant agreement No. 895139 and MSDAvenir research grant (MEKANOS project).

## 6. References

1. P. Clézardin, R. Coleman, M. Puppo, P. Ottewell, E. Bonnelye, F. Paycha, C. B. Confavreux, I. Holen, Bone metastasis: mechanisms, therapies, and biomarkers. *Physiol. Rev.* **101**, 797–855 (2021).
2. C. B. Confavreux, H. Follet, D. Mitton, J. B. Pialat, P. Clézardin, Fracture Risk Evaluation of Bone Metastases: A Burning Issue. *Cancers (Basel)*. **13**, 5711 (2021).
3. F. Eggermont, G. van der Wal, P. Westhoff, A. Laar, M. de Jong, T. Rozema, H. M. Kroon, O. Ayu, L. Derikx, S. Dijkstra, N. Verdonshot, Y. van der Linden, E. Tanck, Patient-specific finite element computer models improve fracture risk assessments in cancer patients with femoral bone metastases compared to clinical guidelines. *Bone*. **130**, 115101 (2020).
4. R. U. Ashford, R. L. Randall, "Bone Metastases: Epidemiology and Societal Effect" in *Metastatic Bone Disease* (Springer New York, 2016; [http://10.0.3.239/978-1-4614-5662-9\\_1](http://10.0.3.239/978-1-4614-5662-9_1)), pp. 3–11.
5. M. Najafi, B. Farhood, K. Mortezaee, Extracellular matrix (ECM) stiffness and degradation as cancer drivers. *J. Cell. Biochem.* **120**, 2782–2790 (2019).
6. P. Lu, V. M. Weaver, Z. Werb, The extracellular matrix: A dynamic niche in cancer progression. *J. Cell Biol.* **196**, 395–406 (2012).
7. V. Gkretsi, T. Stylianopoulos, Cell Adhesion and Matrix Stiffness: Coordinating Cancer Cell Invasion and Metastasis. *Front. Oncol.* **8**, 145 (2018).
8. M. Plodinec, M. Loparic, C. A. Monnier, E. C. Obermann, R. Zanetti-Dallenbach, P. Oertle, J. T. Hyotyla, U. Aebi, M. Bentires-Alj, R. Y. H. Lim, C.-A. Schoenenberger, The nanomechanical signature of breast cancer. *Nat. Nanotechnol.* **7**, 757–765 (2012).
9. G. K. Katara, A. Kulshrestha, L. Mao, X. Wang, M. Sahoo, S. Ibrahim, S. Pamarthy, K. Suzue, G. S. Shekhawat, A. Gilman-Sachs, K. D. Beaman, Mammary epithelium-specific inactivation of V-ATPase reduces stiffness of extracellular matrix and enhances metastasis of breast cancer. *Mol. Oncol.* **12**, 208–223 (2018).
10. A. Samani, J. Zubovits, D. Plewes, Elastic moduli of normal and pathological human breast

- tissues: an inversion-technique-based investigation of 169 samples. *Phys. Med. Biol.* **52**, 1565–1576 (2007).
11. A. Ansardamavandi, M. Tafazzoli-Shadpour, R. Omidvar, I. Jahanzad, Quantification of effects of cancer on elastic properties of breast tissue by Atomic Force Microscopy. *J. Mech. Behav. Biomed. Mater.* **60**, 234–242 (2016).
  12. T. A. Krouskop, T. M. Wheeler, F. Kallel, B. S. Garra, T. Hall, Elastic Moduli of Breast and Prostate Tissues under Compression. *Ultrason. Imaging.* **20**, 260–274 (1998).
  13. J. Fenner, A. C. Stacer, F. Winterroth, T. D. Johnson, K. E. Luker, G. D. Luker, Macroscopic Stiffness of Breast Tumors Predicts Metastasis. *Sci. Rep.* **4** (2015), doi:10.1038/srep05512.
  14. J. W. Lee, E. I. S. Lorenzo, B. Ahn, C. K. Oh, H.-J. Kim, W. K. Han, J. Kim, K. H. Rha, Palpation Device for the Identification of Kidney and Bladder Cancer: A Pilot Study. *Yonsei Med. J.* **52**, 768 (2011).
  15. A. Lyshchik, T. Higashi, R. Asato, S. Tanaka, J. Ito, M. Hiraoka, A. B. Brill, T. Saga, K. Togashi, Elastic Moduli of Thyroid Tissues under Compression. *Ultrason. Imaging.* **27**, 101–110 (2005).
  16. R. W. Tilghman, C. R. Cowan, J. D. Mih, Y. Koryakina, D. Gioeli, J. K. Slack-Davis, B. R. Blackman, D. J. Tschumperlin, J. T. Parsons, Matrix Rigidity Regulates Cancer Cell Growth and Cellular Phenotype. *PLoS One.* **5**, e12905 (2010).
  17. M. Tian, Y. Li, W. Liu, L. Jin, X. Jiang, X. Wang, Z. Ding, Y. Peng, J. Zhou, J. Fan, Y. Cao, W. Wang, Y. Shi, The nanomechanical signature of liver cancer tissues and its molecular origin. *Nanoscale.* **7**, 12998–13010 (2015).
  18. H. Abramczyk, A. Imiela, The biochemical, nanomechanical and chemometric signatures of brain cancer. *Spectrochim. Acta Part A Mol. Biomol. Spectrosc.* **188**, 8–19 (2018).
  19. A. Ansardamavandi, M. Tafazzoli-Shadpour, R. Omidvar, F. Nili, <p>An AFM-Based Nanomechanical Study of Ovarian Tissues with Pathological Conditions</p>. *Int. J. Nanomedicine.* **Volume 15**, 4333–4350 (2020).
  20. X. Wang, J. Wang, Y. Liu, H. Zong, X. Che, W. Zheng, F. Chen, Z. Zhu, D. Yang, X. Song, Alterations in mechanical properties are associated with prostate cancer progression. *Med. Oncol.* **31** (2014), doi:10.1007/s12032-014-0876-9.
  21. A. Elosegui-Artola, The extracellular matrix viscoelasticity as a regulator of cell and tissue dynamics. *Curr. Opin. Cell Biol.* **72**, 10–18 (2021).
  22. A. G. Clark, A. Maitra, C. Jacques, A. Simon, C. Pérez-González, X. Trepas, R. Voituriez, D. M. Vignjevic, “Viscoelastic relaxation of collagen networks provides a self-generated directional cue during collective migration” (Cold Spring Harbor Laboratory, 2020), , doi:10.1101/2020.07.11.198739.
  23. Y. M. Efremov, T. Okajima, A. Raman, Measuring viscoelasticity of soft biological samples using atomic force microscopy. *Soft Matter.* **16**, 64–81 (2020).
  24. J. E. Sader, J. R. Friend, Note: Calibration of atomic force microscope cantilevers using only their resonant frequency and quality factor. *Rev. Sci. Instrum.* **85**, 116101 (2014).
  25. H. Schillers, C. Rianna, J. Schäpe, T. Luque, H. Doschke, M. Wälte, J. J. Uriarte, N. Campillo, G. P. A. Michanetzis, J. Bobrowska, A. Dumitru, E. T. Herruzo, S. Bovio, P. Parot, M. Galluzzi, A. Podestà, L. Puricelli, S. Scheuring, Y. Missirlis, R. Garcia, M. Odorico, J.-M. Teulon, F. Lafont, M. Lekka, F. Rico, A. Rigato, J.-L. Pellequer, H. Oberleithner, D. Navajas, M. Radmacher, Standardized Nanomechanical Atomic Force Microscopy Procedure (SNAP) for Measuring Soft

- and Biological Samples. *Sci. Rep.* **7** (2017), doi:10.1038/s41598-017-05383-0.
26. K. Heinze, O. Arnould, J.-Y. Delenne, V. Lullien-Pellerin, M. Ramonda, M. George, On the effect of local sample slope during modulus measurements by contact-resonance atomic force microscopy. *Ultramicroscopy.* **194**, 78–88 (2018).
  27. D.-M. Kaimaki, B. E. Smith, C. Durkan, On the use of nanomechanical atomic force microscopy to characterise oil-exposed surfaces. *RSC Adv.* **8**, 6680–6689 (2018).
  28. F. Rico, P. Roca-Cusachs, N. Gavara, R. Farré, M. Rotger, D. Navajas, Probing mechanical properties of living cells by atomic force microscopy with blunted pyramidal cantilever tips. *Phys. Rev. E.* **72** (2005), doi:10.1103/physreve.72.021914.
  29. M. L. Oyen, Spherical indentation creep following ramp loading. *J. Mater. Res.* **20**, 2094–2100 (2005).
  30. M. L. Oyen, Analytical techniques for indentation of viscoelastic materials. *Philos. Mag.* **86**, 5625–5641 (2006).
  31. J. M. Mattice, A. G. Lau, M. L. Oyen, R. W. Kent, Spherical indentation load-relaxation of soft biological tissues. *J. Mater. Res.* **21**, 2003–2010 (2006).
  32. S. Qiu, X. Zhao, J. Chen, J. Zeng, S. Chen, L. Chen, Y. Meng, B. Liu, H. Shan, M. Gao, Y. Feng, Characterizing viscoelastic properties of breast cancer tissue in a mouse model using indentation. *J. Biomech.* **69**, 81–89 (2018).
  33. K. S. S. Bhatia, C. S. L. Tong, C. C. M. Cho, E. H. Y. Yuen, Y. Y. P. Lee, A. T. Ahuja, Shear wave elastography of thyroid nodules in routine clinical practice: preliminary observations and utility for detecting malignancy. *Eur. Radiol.* **22**, 2397–2406 (2012).
  34. B. Piersma, M.-K. Hayward, V. M. Weaver, Fibrosis and cancer: A strained relationship. *Biochim. Biophys. Acta - Rev. Cancer.* **1873**, 188356 (2020).
  35. E. Massy, J. C. Rousseau, M. Gueye, E. Bonnelye, M. Brevet, L. Chambard, M. Duruisseaux, O. Borel, C. Roger, R. Guelminger, J. B. Pialat, E. Gineyts, L. Bouazza, M. Millet, J. M. Maury, P. Clézardin, N. Girard, C. B. Confavreux, Serum total periostin is an independent marker of overall survival in bone metastases of lung adenocarcinoma. *J. Bone Oncol.* **29**, 100364 (2021).
  36. A. J. van der Slot-Verhoeven, E. A. van Dura, J. Attema, B. Blauw, J. DeGroot, T. W. J. Huizinga, A.-M. Zuurmond, R. A. Bank, The type of collagen cross-link determines the reversibility of experimental skin fibrosis. *Biochim. Biophys. Acta - Mol. Basis Dis.* **1740**, 60–67 (2005).
  37. M. W. Pickup, H. Laklai, I. Acerbi, P. Owens, A. E. Gorska, A. Chytil, M. Aakre, V. M. Weaver, H. L. Moses, Stromally Derived Lysyl Oxidase Promotes Metastasis of Transforming Growth Factor- $\beta$ -Deficient Mouse Mammary Carcinomas. *Cancer Res.* **73**, 5336–5346 (2013).
  38. I. Acerbi, L. Cassereau, I. Dean, Q. Shi, A. Au, C. Park, Y. Y. Chen, J. Liphardt, E. S. Hwang, V. M. Weaver, Human breast cancer invasion and aggression correlates with ECM stiffening and immune cell infiltration. *Integr. Biol.* **7**, 1120–1134 (2015).
  39. B. Xu, R. Ghossein, Poorly differentiated thyroid carcinoma. *Semin. Diagn. Pathol.* **37**, 243–247 (2020).
  40. M. Ragazzi, A. Ciarrocchi, V. Sancisi, G. Gandolfi, A. Bisagni, S. Piana, Update on Anaplastic Thyroid Carcinoma: Morphological, Molecular, and Genetic Features of the Most Aggressive Thyroid Cancer. *Int. J. Endocrinol.* **2014**, 1–13 (2014).
  41. M. Daugherty, D. Sedaghatpour, O. Shapiro, S. Vourganti, A. Kutikov, G. Bratslavsky, *Urol.*

- Oncol.*, in press, doi:10.1016/j.urolonc.2016.11.009.
42. R. Sinkus, M. Tanter, T. Xydeas, S. Catheline, J. Bercoff, M. Fink, Viscoelastic shear properties of in vivo breast lesions measured by MR elastography. *Magn. Reson. Imaging*. **23**, 159–165 (2005).
  43. P. Garteiser, S. Doblus, J.-L. Daire, M. Wagner, H. Leitao, V. Vilgrain, R. Sinkus, B. E. Van Beers, MR elastography of liver tumours: value of viscoelastic properties for tumour characterisation. *Eur. Radiol.* **22**, 2169–2177 (2012).
  44. S. D. Salinas, M. M. Clark, R. Amini, The effects of  $-80^{\circ}\text{C}$  short-term storage on the mechanical response of tricuspid valve leaflets. *J. Biomech.* **98**, 109462 (2020).
  45. N. P. Quirk, C. Lopez De Padilla, R. E. De La Vega, M. J. Coenen, A. Tovar, C. H. Evans, S. A. Müller, Effects of freeze-thaw on the biomechanical and structural properties of the rat Achilles tendon. *J. Biomech.* **81**, 52–57 (2018).
  46. C. Wex, A. Stoll, M. Fröhlich, S. Arndt, H. Lippert, Mechanics of fresh, frozen-thawed and heated porcine liver tissue. *Int. J. Hyperth.* **30**, 271–283 (2014).
  47. B. D. Stemper, N. Yoganandan, M. R. Stineman, T. A. Gennarelli, J. L. Baisden, F. A. Pintar, Mechanics of Fresh, Refrigerated, and Frozen Arterial Tissue. *J. Surg. Res.* **139**, 236–242 (2007).
  48. A. Santago II, A. Kemper, C. McNally, J. Sparks, S. Duma, Freezing affects the mechanical properties of bovine liver. *Biomed. Sci. Instrum.* **45**, 24–29 (2009).
  49. E. A. Kennedy, D. S. Tordonado, S. M. Duma, Effects of freezing on the mechanical properties of articular cartilage. *Biomed. Sci. Instrum.* **43**, 342–347 (2007).
  50. M. Ekiert, J. Karbowniczek, U. Stachewicz, A. Mlyniec, The effect of multiple freeze-thaw cycles on the viscoelastic properties and microstructure of bovine superficial digital flexor tendon. *J. Mech. Behav. Biomed. Mater.* **120**, 104582 (2021).
  51. A. Levillain, S. Ahmed, D.-M. Kaimaki, S. Schuler, S. Barros, D. Labonte, J. Iatridis, N. Nowlan, Prenatal muscle forces are necessary for vertebral segmentation and disc structure, but not for notochord involution in mice. *Eur. Cells Mater.* **41**, 558–575 (2021).
  52. C. Liu, M. Li, Z.-X. Dong, D. Jiang, X. Li, S. Lin, D. Chen, X. Zou, X.-D. Zhang, G. D. Luker, Heterogeneous microenvironmental stiffness regulates pro-metastatic functions of breast cancer cells. *Acta Biomater.* **131**, 326–340 (2021).
  53. J.-L. Gennisson, T. Deffieux, M. Fink, M. Tanter, Ultrasound elastography: Principles and techniques. *Diagn. Interv. Imaging*. **94**, 487–495 (2013).
  54. Z. Yin, T. M. Schmid, T. K. Yasar, Y. Liu, T. J. Royston, R. L. Magin, Mechanical Characterization of Tissue-Engineered Cartilage Using Microscopic Magnetic Resonance Elastography. *Tissue Eng. Part C Methods*. **20**, 611–619 (2014).
  55. S. F. Othman, H. Xu, T. J. Royston, R. L. Magin, Microscopic magnetic resonance elastography ( $\mu\text{MRE}$ ). *Magn. Reson. Med.* **54**, 605–615 (2005).
  56. J. E. L. Jordan, G. Bertalan, T. Meyer, H. Tzschätzsch, A. Gauert, L. Bramè, H. Herthum, Y. Safraou, L. Schröder, J. Braun, A. I. H. Hagemann, I. Sack, Microscopic multifrequency MR elastography for mapping viscoelasticity in zebrafish. *Magn. Reson. Med.* (2021), doi:10.1002/mrm.29066.

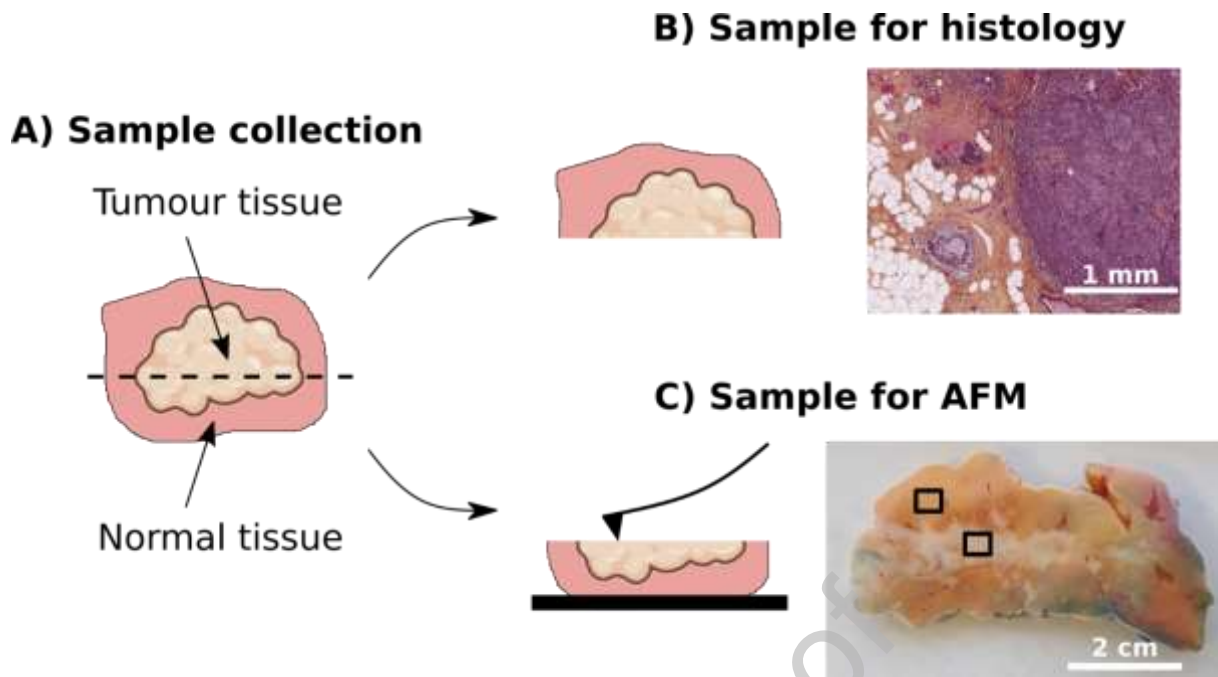


Figure 1 - Sample preparation. A) Human samples containing normal and tumour tissue were collected and divided into two samples. B) One sample was used for histology, as part of the routine pathological diagnosis. C) One sample was used for AFM. The photograph shows a breast sample and the black boxes indicate where the AFM measurements were performed.

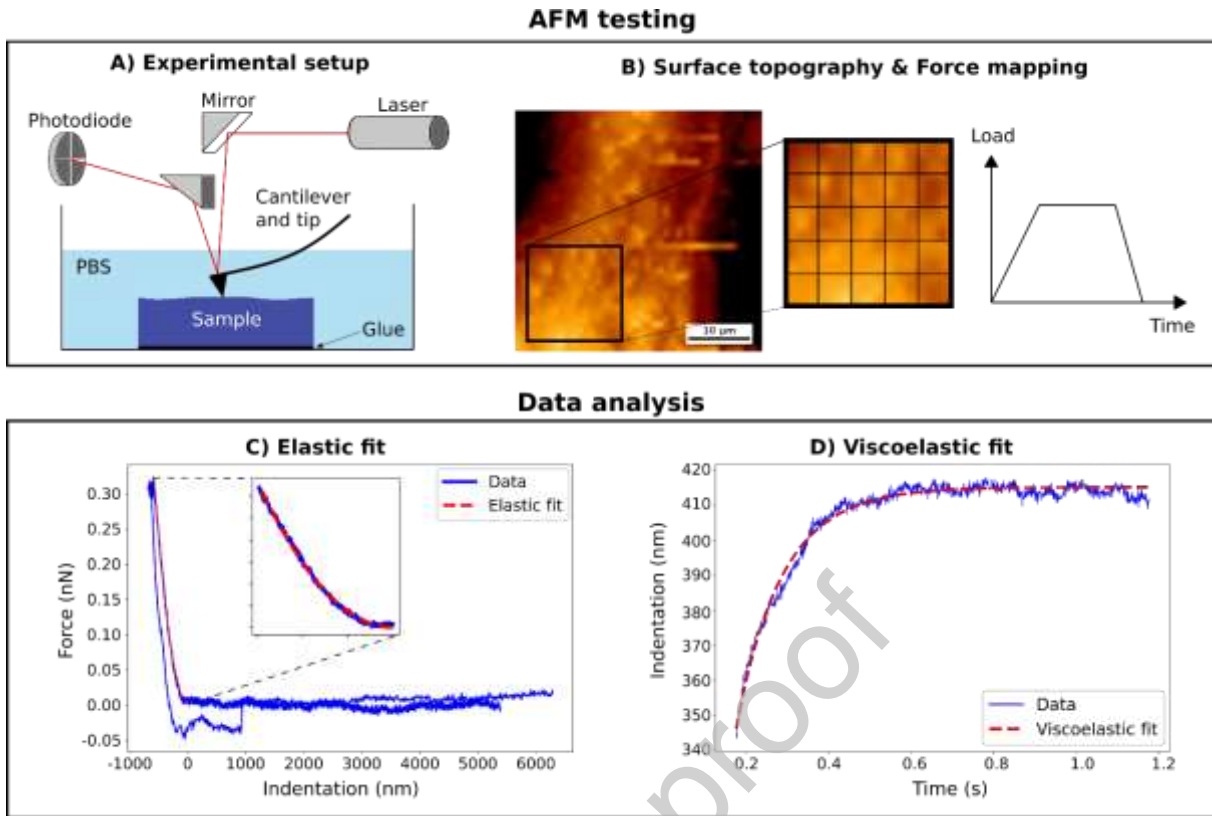


Figure 2 - Method overview for the mechanical characterisation. A) Schematic of the AFM setup. The sample was glued on a petri dish, immersed in PBS and placed on the AFM scanner. B) The AFM tapping mode topography was first used to get the surface profile and identify a region of interest (black box). The force mapping mode was then used in this region of interest with a trapezoidal loading profile. C) Typical force-indentation curve obtained from AFM measurements (blue). Elastic modulus was obtained by fitting the extend segment using Hertz model (red). D) Typical Indentation-time curve on the holding segment (blue). Elastic fraction was obtained by fitting the holding segment using Maxwell model (red).

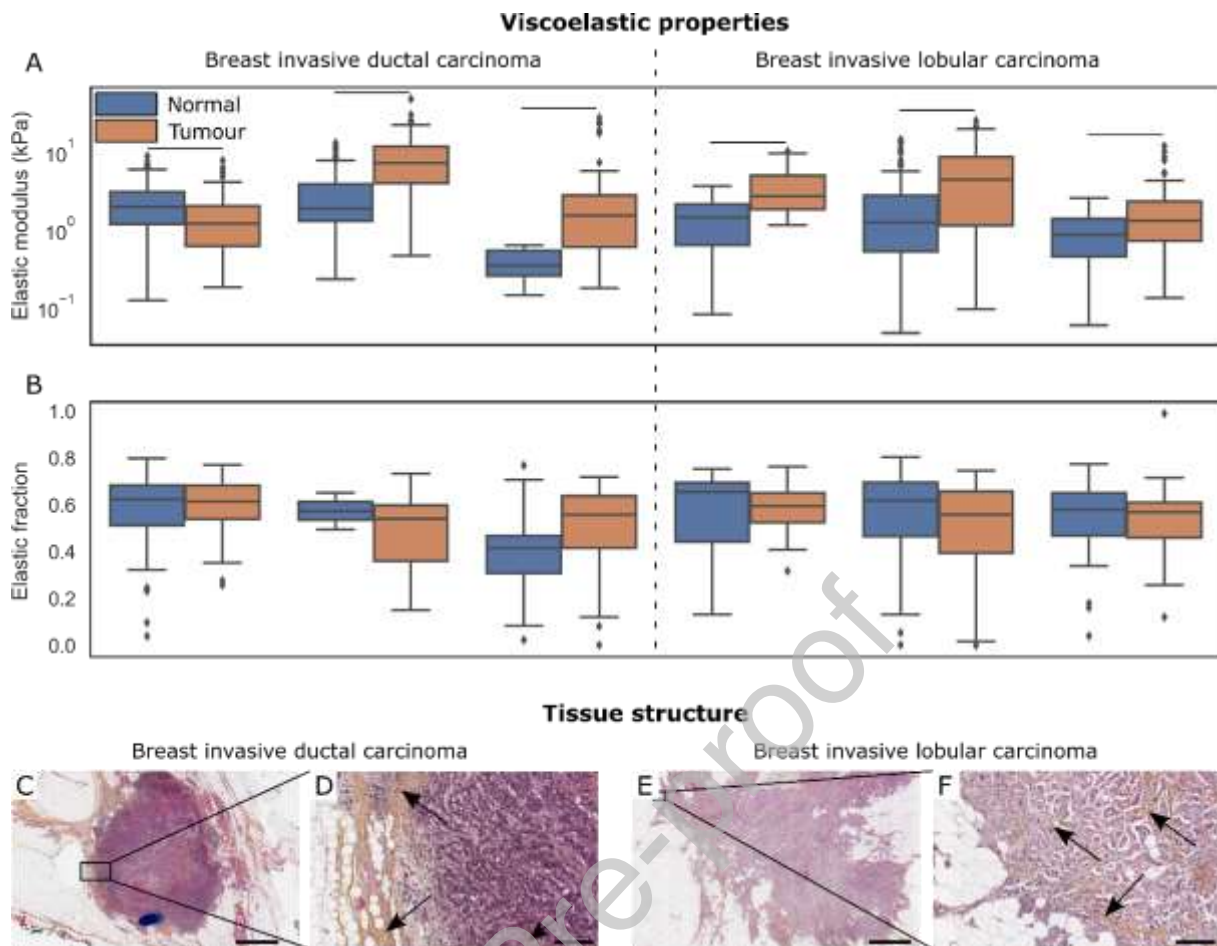


Figure 3 – Breast tumour samples, which were composed of dense fibrous tissue, displayed an increased elastic modulus compared to their normal counterpart. Viscoelastic properties and histopathological examination of breast tumour tissue. A) Elastic modulus and B) elastic fraction of normal (blue) and tumour (orange) tissue for two types of breast cancers and different patients. Horizontal bar indicates significant difference between normal and tumour samples. C-F) Hematoxylin eosin saffron stained sections of breast tumour tissue of each type. Tumour tissue appears in purple, while normal adipose tissue appears in white. Arrows indicate fibrotic tissue. Scale bars: 2 mm (C, E) and 200  $\mu\text{m}$  (D, F).

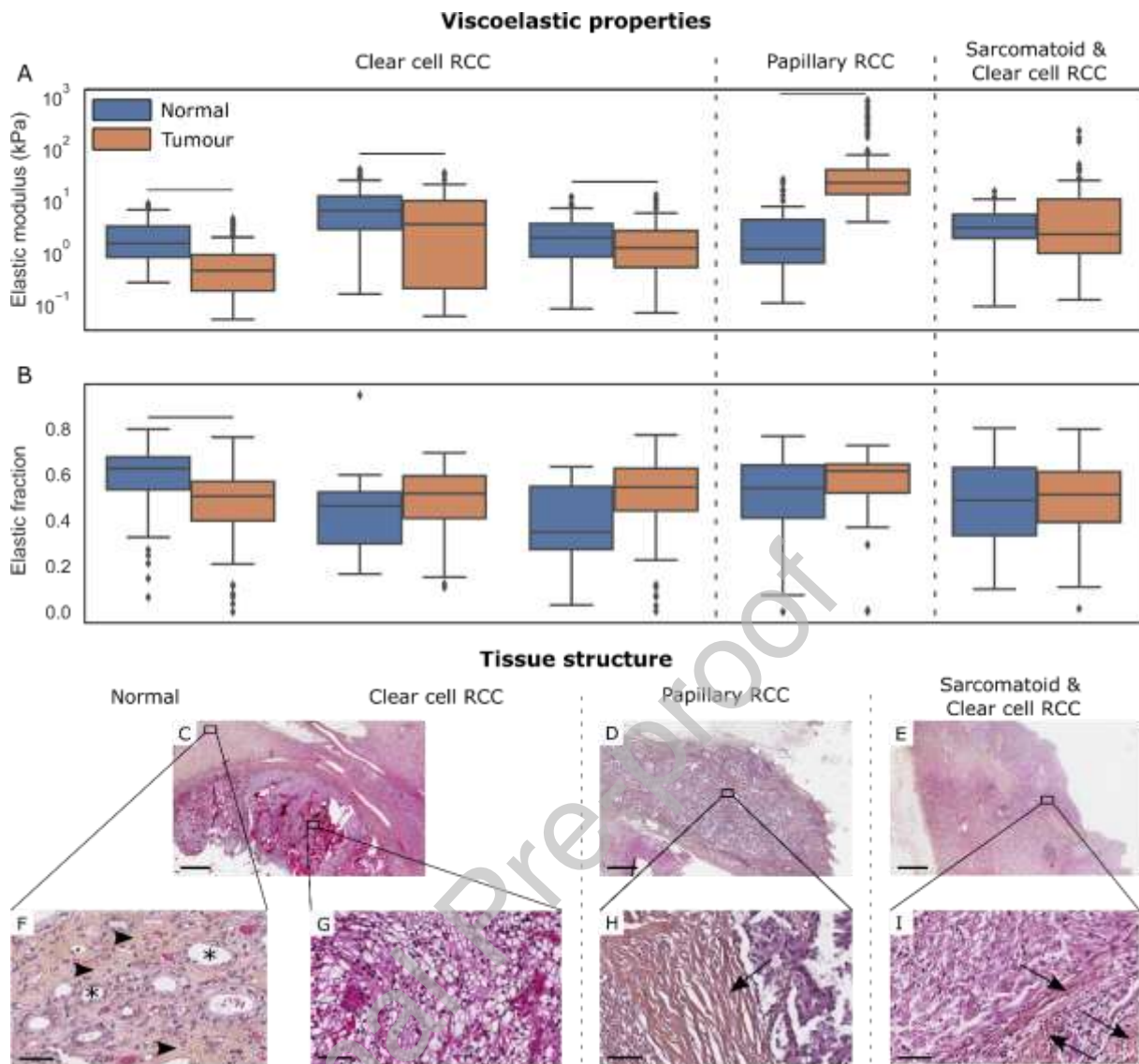


Figure 4 – Elastic properties of kidney tumour samples were differently affected depending on their histological type. Viscoelastic properties and histopathological examination of renal tumour tissue. A) Elastic modulus and B) elastic fraction of normal (blue) and tumour (orange) tissue for three types of kidney cancers and different patients. Horizontal bar indicates significant difference between normal and tumour samples. C-I) Hematoxylin eosin saffron stained sections of kidney normal (C, F) and tumour (C-E, G-I) tissue of each type. Renal tubes (asterisk), connective tissue (arrowhead), and fibrotic tissue (arrow) are indicated. RCC: Renal Cell Carcinoma. Scale bars: 2 mm (C, E) and 60  $\mu$ m (D, F).

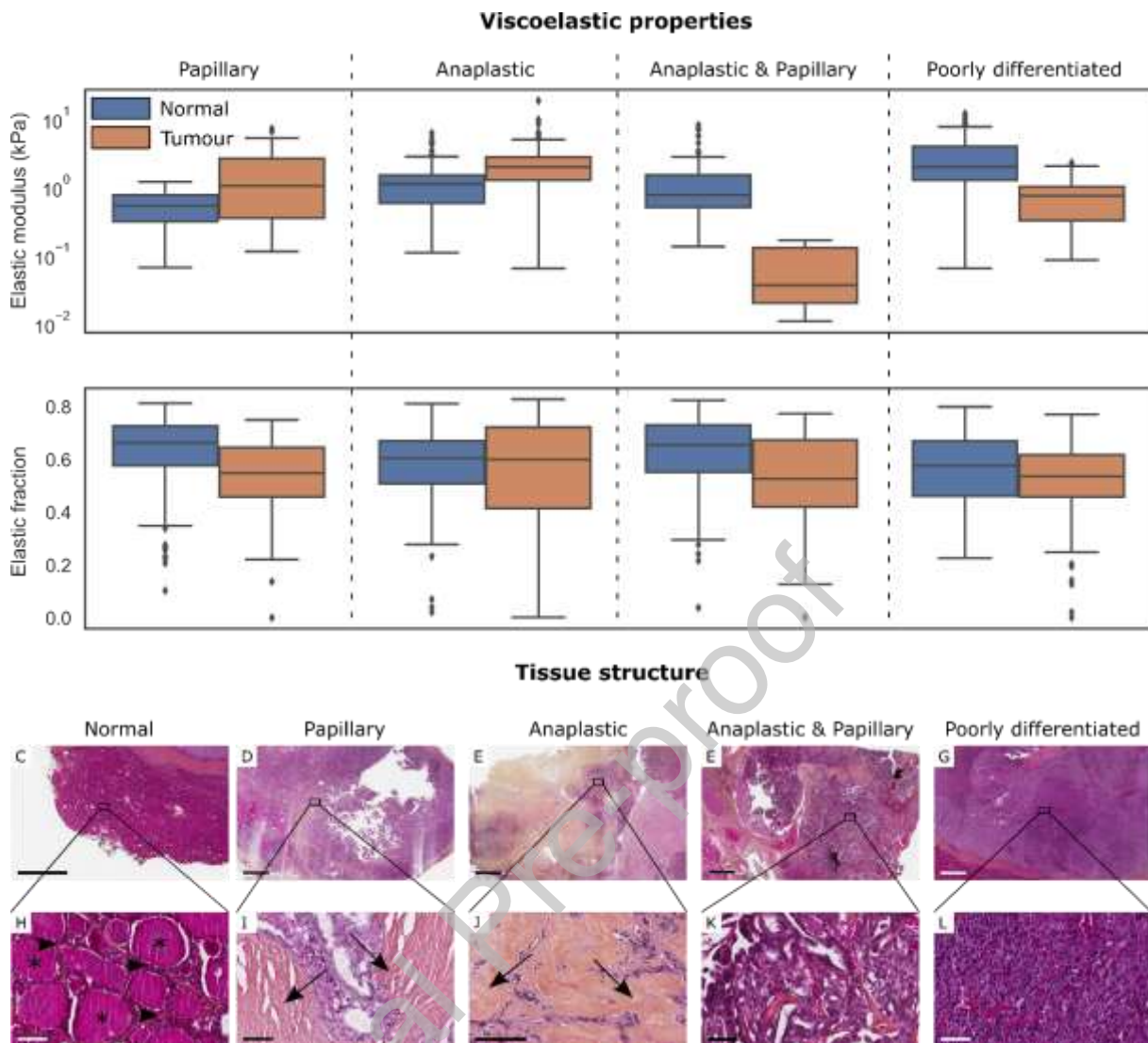


Figure 5 – Elastic properties of thyroid tumour samples were differently affected depending on their histological type, while the elastic fraction tended to decrease in most tumour samples. Viscoelastic properties and histopathological examination of thyroid tumour tissue. A) Elastic modulus and B) elastic fraction of normal (blue) and tumour (orange) tissue for different types of thyroid cancers. Horizontal bar indicates significant difference between normal and tumour samples. C-L) Hematoxylin eosin saffron stained sections of thyroid normal (C, H) and tumour (D-G, I, L) tissue. Colloid fluid (asterisk), connective tissue (arrowhead) and fibrotic tissue (arrow) are indicated. Scale bars: 2 mm (C-G) and 60  $\mu\text{m}$  (H-L).

Breast						
Sample #	Type	Group	Elastic modulus (kPa)		Elastic fraction	
			Mean $\pm$ Std	Median	Mean $\pm$ Std	Median
1	NST	Normal	2.4 $\pm$ 1.7	2.0	0.58 $\pm$ 0.16	0.62
		Tumour	1.5 $\pm$ 1.3	1.2	0.60 $\pm$ 0.10	0.61
			<b>p &lt; 0.001</b>		p = 0.78	
2	NST	Normal	3.2 $\pm$ 3.0	1.9	0.57 $\pm$ 0.11	0.57
		Tumour	8.5 $\pm$ 6.7	7.2	0.48 $\pm$ 0.16	0.54
			<b>p &lt; 0.001</b>		p = 0.42	
3	NST	Normal	0.37 $\pm$ 0.16	0.35	0.40 $\pm$ 0.16	0.41
		Tumour	2.7 $\pm$ 4.4	1.5	0.50 $\pm$ 0.17	0.56
			<b>p &lt; 0.001</b>		<b>p &lt; 0.001</b>	
4	ILC	Normal	1.4 $\pm$ 0.90	1.4	0.56 $\pm$ 0.18	0.66
		Tumour	3.7 $\pm$ 2.8	2.7	0.58 $\pm$ 0.14	0.60
			<b>p &lt; 0.001</b>		p = 0.88	
5	ILC	Normal	2.5 $\pm$ 3.2	1.2	0.56 $\pm$ 0.19	0.62
		Tumour	5.9 $\pm$ 5.6	4.4	0.51 $\pm$ 0.19	0.60
			<b>p &lt; 0.001</b>		p = 0.068	
6	ILC	Normal	0.93 $\pm$ 0.64	0.85	0.53 $\pm$ 0.17	0.58
		Tumour	1.9 $\pm$ 2.1	1.3	0.54 $\pm$ 0.20	0.60
			<b>p &lt; 0.001</b>		p = 0.70	

Table 1 – Elastic modulus and elastic fraction of normal and tumour tissue for each breast sample.

Results are indicated as mean  $\pm$  standard deviation (std) and median. The p values show differences between normal and tumour tissue for each sample. NST: No Special type; ILC: Invasive Lobular Carcinoma.

Kidney						
Sample #	Type	Group	Elastic modulus (kPa)		Elastic fraction	
			Mean $\pm$ Std	Median	Mean $\pm$ Std	Median
1	CC	Normal	2.2 $\pm$ 1.9	1.5	0.59 $\pm$ 0.14	0.63
		Tumour	0.75 $\pm$ 0.85	0.44	0.47 $\pm$ 0.16	0.51
			<b>p &lt; 0.001</b>		<b>p &lt; 0.001</b>	
2	CC	Normal	8.9 $\pm$ 8.4	6.3	0.44 $\pm$ 0.22	0.46
		Tumour	6.7 $\pm$ 8.8	3.5	0.47 $\pm$ 0.17	0.52
			<b>p = 0.0073</b>		p = 0.33	
3	CC	Normal	2.8 $\pm$ 3.0	1.9	0.37 $\pm$ 0.21	0.35
		Tumour	1.9 $\pm$ 2.1	1.2	0.51 $\pm$ 0.17	0.55
			<b>p = 0.028</b>		p = 0.055	
4	P	Normal	3.0 $\pm$ 4.5	1.1	0.49 $\pm$ 0.20	0.54
		Tumour	67 $\pm$ 139	21	0.55 $\pm$ 0.17	0.62
			<b>p &lt; 0.001</b>		p = 0.17	
5	CC-S	Normal	3.9 $\pm$ 3.2	2.9	0.47 $\pm$ 0.19	0.49
		Tumour	15 $\pm$ 36	2.2	0.49 $\pm$ 0.16	0.51
			<b>p = 0.79</b>		p = 0.77	

Table 2 – Elastic modulus and elastic fraction of normal and tumour tissue for each kidney sample.

Results are indicated as mean  $\pm$  standard deviation (std) and median. The p values show differences between normal and tumour tissue for each sample. CC: Clear Cell renal cell carcinoma; P: Papillary carcinoma; CC-S: Clear Cell and Sarcomatoid carcinoma.

Thyroid						
Sample #	Type	Group	Elastic modulus (kPa)		Elastic fraction	
			Mean $\pm$ Std	Median	Mean $\pm$ Std	Median
1	P	Normal	0.54 $\pm$ 0.28	0.53	0.62 $\pm$ 0.15	0.66
		Tumour	1.7 $\pm$ 1.7	1.0	0.52 $\pm$ 0.17	0.55
			<b>p &lt; 0.001</b>		<b>p &lt; 0.001</b>	
2	A	Normal	1.3 $\pm$ 1.0	1.1	0.56 $\pm$ 0.16	0.61
		Tumour	2.4 $\pm$ 2.2	2.0	0.56 $\pm$ 0.20	0.60
			<b>p &lt; 0.001</b>		p = 0.55	
3	P-A	Normal	1.4 $\pm$ 1.6	0.77	0.61 $\pm$ 0.18	0.65
		Tumour	0.070 $\pm$ 0.056	0.036	0.50 $\pm$ 0.21	0.53
			<b>p &lt; 0.001</b>		<b>p = 0.016</b>	
4	PD	Normal	2.9 $\pm$ 2.5	2.0	0.55 $\pm$ 0.15	0.58
		Tumour	0.78 $\pm$ 0.54	0.74	0.50 $\pm$ 0.17	0.54
			<b>p &lt; 0.001</b>		p = 0.17	

Table 3 – Elastic modulus and elastic fraction of normal and tumour tissue for each thyroid sample.

Results are indicated as mean  $\pm$  standard deviation (std) and median. The p values show differences between normal and tumour tissue for each sample. P: Papillary carcinoma; A: Anaplastic carcinoma; P-A: Papillary and Anaplastic carcinoma; PD: Poorly Differentiated carcinoma.